Metastable aluminium atoms floating on the surface of helium nanodroplets.

Jay Jeffs[1], Nicholas A. Besley[1] and Anthony J. Stace[1*]
Gautam Sarma[2], Ethan M. Cunningham[2], Adrian Boatwright[2], Shengfu Yang[2], and Andrew M. Ellis[2]
[1]*Department of Physical and Theoretical Chemistry, School of Chemistry, The University of Nottingham, University Park, Nottingham NG7 2RD, U.K.*
[2]*Department of Chemistry, University of Leicester, Leicester LE1 7RH, U.K.*

Metal atoms have proved to be sensitive probes of the properties of superfluid helium nanodroplets. To date, all experiments on the doping of helium droplets have concentrated on the attachment of metal atoms in their ground electronic states. Here we report the first examples of metal atoms in excited states becoming attached to helium nanodroplets. The atoms in question are aluminium and they have been generated by laser ablation in a metastable quartet state, which attaches to and remains on the surface of helium droplets. Evidence for a surface location comes from electronic spectra, which consist of very narrow absorption profiles that show very small spectral shifts. Supporting *ab initio* calculations show there to be an energy incentive for a metastable Al atom to remain on the surface of a helium droplet rather than move to the interior. The results suggest that helium droplets may provide a method for the capture and transport of metastable excited atomic and molecular species.

tony.stace@nottingham.ac.uk

From their onset, experiments on doped helium nanodroplets have paid considerable attention to the spectroscopy of single atoms, since the associated shifts and widths of electronic spectral features have been found to be sensitive to whether an atom is located inside or on the surface of a droplet [1-4]. There appears to be general agreement that alkali metal atoms reside on the surfaces of droplets [5,6], as do several of the alkaline earth metals

[7-13]. Almost all such studies have concentrated on metal atoms with either no or one unpaired electron and these have been added to the droplets in their electronic ground state; the only higher spin systems that have been investigated are chromium atoms, weakly bound alkali dimers and trimers, and the silver dimer [14-18].

Reported here are results from experiments where aluminium atoms have been ablated by laser from a solid sample of the metal in the presence of helium nanodroplets. From these experiments the presence of metastable aluminium atoms in the ^{4}P ($3s3p^2$) state at ~29,000cm^{-1} above the ground state [19-21] has been established through observation of a series of 13 separate electronic transitions originating from this electronic state. In complete contrast to almost all previous studies, the wavelengths at which spectral transitions are recorded for these metal atoms in helium droplets exhibit almost no shift from those measured in the gas phase [19]. Transitions involving the metastable ^{4}P states also exhibit comparatively narrow linewidths, which is again very unusual for helium nanodroplets. Narrow linewidths have been reported previously [14,22] and in some cases interpreted as being due to a very weak interaction between the metal atom and the surrounding helium atoms [22].

There has been one previous study of the electronic transitions of aluminium atoms in helium droplets, by Reho *et al.* [23]. These authors identified two very broad absorption features (FWHM ~ 420 cm^{-1}) that were assigned to transitions from the ^{2}P ground state to the lowest ^{2}D excited state and the authors concluded that spin-orbit coupling in the ^{2}D state is quenched by the helium [23]. Previous observations of the spectra of alkali atoms in bulk helium have been interpreted in terms of a mechanism whereby excited spin-orbit states undergo rapid non-radiative relaxation to the lowest (Ω = 1/2) level [24]. In contrast, the spectra presented here involve a number of spin-orbit states of electronically excited Al and there is no evidence of quenching. With the current high level of interest both in Rydberg

atoms and their coherent control and the physics of ultra-cold atoms, state selectivity on the part of helium nanodroplets may provide a mechanism for generating and transporting excited atomic species.

The two instruments employed in these experiments use very similar methods to prepare helium droplets, but differ with regard to the technique used to record photoionization signals from Al atoms. Fig. 1 shows a generic overview of the apparatus and further details of how each experiment has been undertaken can be found in the Supplementary Information. Photoionization spectra between 42,000 and 44,000 cm^{-1} have been recorded by monitoring Al^+ signals as a function of laser wavelength following metal ablation in three separate regions of the apparatus. To establish which electronic states are being produced during laser vaporization, Fig. 2a shows a spectrum recorded from isolated Al atoms ionized under gas phase conditions in the ion source of the reflectron (region 3 in figure 1). Fig.2b shows the same scan range, but recorded from Al atoms ablated in the expansion region of the cooled nozzle (region 1 in figure 1 where helium droplets containing 10^3-10^4 helium atoms were being formed). Note the three transitions seen in Fig. 2a at ~ 42120 and ~42230 cm^{-1} that are known to originate from aluminium atoms in the ground state [19], disappear in Fig. 2b due to spectral shifts identified by Reho *et al.* [23]. With the latter transitions omitted, two separate scans between 42,000 and 44,000 cm^{-1} show a total of 13 transitions associated with Al ablated in region 1 (see Fig. S5 for a complete scan). A search of known electronic transitions in aluminium atoms that, with a single photon, would place atoms above the lowest ionization limit (48,278.37 cm^{-1}) at the energies covered [19-21], suggests that all of the transitions shown in Fig. 2b originate from spin-orbit sub-states derived from the Al ^4P ($3s3p^2$) state, which lies approximately 29,000 cm^{-1} above the ground state. This state of Al is metastable because transitions to the ground electronic state are forbidden by both orbital and spin angular momentum selection rules, and thus a relatively

long radiative lifetime is anticipated. One-photon transitions out of the ^{4}P state would place the atoms in Rydberg states lying at ~71,000 cm^{-1} from where they could undergo autoionization. Similar sharp features seen in the UV spectra of sputtered silver atoms have been attributed to one-photon excitation from a metastable state of Ag I to a series of Rydberg states that subsequently autoionised [25].

To verify that the strong Al^+ signals shown in Fig. 2b are associated with the helium droplets and are not from Al atoms becoming entrained in the gas flow, additional spectra were recorded on a second apparatus. Here Al atoms were ablated in the presence of a *collimated* beam of helium nanodroplets (region 2 in figure 1 where droplets contain ~ 10^4 atoms). What characterises these measurements is that it has been possible to monitor the intensities of the adduct ions, $Al^+(He)_n$, as a function of laser wavelength. These results are shown in Fig. 3, where a summation of the intensities of the n = 1-3 signals is compared with measurements of the Al^+ signal recorded under identical circumstances. As can be seen, over the range selected, 42100 - 42225 cm^{-1}, there is an excellent match between the two spectra. Since the beam density in the ionization region is very low, there is no possibility of bare Al^+ ions undergoing the three-body collisions necessary to generate $Al^+(He)_n$ complexes, thus demonstrating that the sharp spectral transitions are indeed due to aluminium atoms attached to helium nanodroplets. Table 1 lists the 13 transitions which have been identified as due to the metastable ^{4}P ($3s3p^2$) state together with their shifts with respect to the gas phase transition energies and their linewidths. The magnitudes of the shifts are all close to the grating/calibration errors; but there appears to be a very small and consistent shift associated with the majority of transitions.

Table II shows the properties of potential energy curves calculated for Al-He$_n$ clusters using CCSD(T) methodology. Details of the calculations are to be found in the Supplementary Information. These calculations are for an aluminium atom in the ^{4}P ($3s3p^2$)

state, which arises from the promotion of one of the electrons from the full 3s orbital in the ground state to an unoccupied 3p orbital in the ^{4}P state. The key difference between this state and the ground electronic state is that there are now two occupied 3p orbitals and one unpaired 3s electron. In the $1^4\Pi$ state of the Al-He dimer there is an electron in the $3p_z$ orbital pointing towards the helium atom and, as Table II shows, the resulting complex has a calculated binding energy of just 4.81 cm^{-1} and an internuclear separation, R_{min}, of 5.38 Å. In contrast in the $1^4\Sigma$ state the $3p_z$ orbital is unoccupied and has a computed well depth of 173.9 cm^{-1}. A similar pattern is observed for Al-He$_2$, where the binding energy per atom remains high. In the Al-He$_4$ complex the quartet state will necessarily have at least one occupied 3p orbital orientated towards a helium atom. Similarly, for Al-He$_6$ the two atoms coordinating in the *z*-direction are again strongly bound, whilst the remaining four atoms bind more weakly. Overall, a consequence of increasing coordination is that the high binding energies seen for the smaller complexes start to decline. However, for Al-He$_6$ the binding energy per helium atom is calculated to be 41.3 cm^{-1}, which is still four times larger than for the corresponding ^{2}P electronic ground state [23]. In a final calculation, the preferred coordination of ground and excited state atoms has been compared in a cluster consisting of 98 helium atoms. From the results shown in Table II it can be seen that ground-state aluminium prefers, by a very small margin, to be at the centre of a droplet, whereas the ^{4}P excited state favours a surface site by the larger margin of 83 cm^{-1}. A significant fraction of this additional stability comes from a strong association between ^{4}P aluminium and a single helium atom. Optimised structures for the clusters with ground and excited state Al atoms are shown in Fig. 4. These results are significant for two reasons; first, the calculations show that in the experiment where excited state atoms become attached to pre-formed helium droplets, the atoms will remain on the surface. Second, in the experiment where excited state atoms are entrained in the helium expansion close to the nozzle (region 1 of Fig. 1), any aluminium atoms solvated

in droplets will have an energy incentive to move to the surface. Overall, the results show that the excited quartet state of the aluminium atom could occupy a comparatively stable site on or close to the surface of a helium droplet, where it would still be more strongly bound than solvated ground state atoms.

The transitions identified in Table I involve all possible spin-orbit levels of the initial state, which implies a complete absence of any of the angular momentum relaxation mechanisms that have been discussed previously for both aluminium in helium droplets and for certain alkali metals in bulk helium [23,24,26]. The latter experiments have linked spin-orbit quenching to the formation of exciplexes, and metals with small spin-orbit splittings, such as Li and Na, seem particularly susceptible [26]. In helium droplets the evidence is somewhat contradictory; surface-bound Na and K atoms not only form exciplexes with small numbers of helium atoms, but there is also an absence of spin-orbit quenching [27,28]. Excited state metal–helium molecular orbitals associated with exciplex formation are exclusively of Π symmetry and excitation to any state with Σ symmetry is assumed to result in desorption of the bare metal atom [29]. In contrast, the strongly-bound dimer state identified here for the ^{4}P Al atoms has Σ symmetry. There is the possibility that diatomic Π state exciplexes involving the $3s3p^2$ state are being expelled from the droplets and then photoionized. However, were that the case, then the subsequent excitation/autoionizing step might have been expected to yield vibrational structure, and that is not seen in either Fig. 2 or Fig. 3.

To account for the observation of the strong Al^+ signal after metastable excitation the following sequence of events is proposed. First, Al atoms in the ^{4}P excited state are assumed to reside on the surface of helium droplets, which is strongly supported by the calculations presented here and by the experimental observation of narrow linewidths and negligible line shifts for spectroscopic transitions relative to the gas phase. Indeed these observations

suggest minimal interaction with the helium. Following photoexcitation, it is proposed that the resultant autoionizing state is expelled from the droplet prior to ionization, which would then ensure that predominantly Al^+ ions are formed in the process. A very similar sequence of events has been proposed by Federmann *et al.* [30] to account for the appearance of narrow absorption features in their Rydberg spectra of silver atoms trapped in helium droplets. However, unlike their system [31], the excited aluminium atoms reported here must undergo discrete excitation to an autoionizing Rydberg state *before* expulsion because the entire process requires just one rather than two photons.

UV photoionization spectra have been recorded from aluminium atoms in a metastable excited electronic state in the presence of a beam of helium nanodroplets, and where the observed transitions exhibit narrow line widths and almost no spectral shift relative to the gas phase. Supporting *ab initio* calculations show that there is an energy incentive for the excited state to reside on the surface of a droplet.

ACKNOWLEDGEMENTS

The authors would like to thank EPSRC and the Leverhulme Trust for financial support and Prof. Tim Wright and Dr. Pascal Lablanquie for a number of helpful comments on the results. The Nuffield Foundation is also thanked for providing a bursary to Ethan Cunningham. Very helpful discussions with Prof. W. H. Breckenridge on metal atom excited states are also acknowledged.

Figure 1. Generic diagram that combines the essential features of the two separate pieces of apparatus used. Regions associated with the three separate experiments undertaken are labelled.

Figure 2. (a) Photoionization spectrum recorded from gas phase ablated Al atoms (region 3 of Fig. 1). Transitions arising from non-resonant two-photon ionization of ground state atoms are denoted by *; (b) Photoionization spectrum recorded from Al atoms ablated into the expansion region of the cooled nozzle (region 1 in figure 1 where helium droplets containing 10^3-10^4 helium atoms were being formed). Both spectra were recorded by monitoring the Al^+ signal in the reflectron and the gas phase spectrum has been shift upwards to avoid any overlap.

Figure 3. Photoionization spectra recorded following the ablation of Al atoms in the presence of a *collimated* beam of helium nanodroplets (region 2 in figure 1 where the droplets contain ~ 10^4 atoms). The spectra were recorded by monitoring the signal from either Al^+ (black line) or $AlHe_n^+$ (by summation of the n = 1-3 signals) (red line).

Figure 4. Optimized structures calculated for an aluminium atom at the centre and at the surface of a 98 atom helium cluster. (a) and (b) are for Al in the electronic ground state and (c) and (d) are for the $3s3p^2$ (^4P) excited state .

Figure 1.

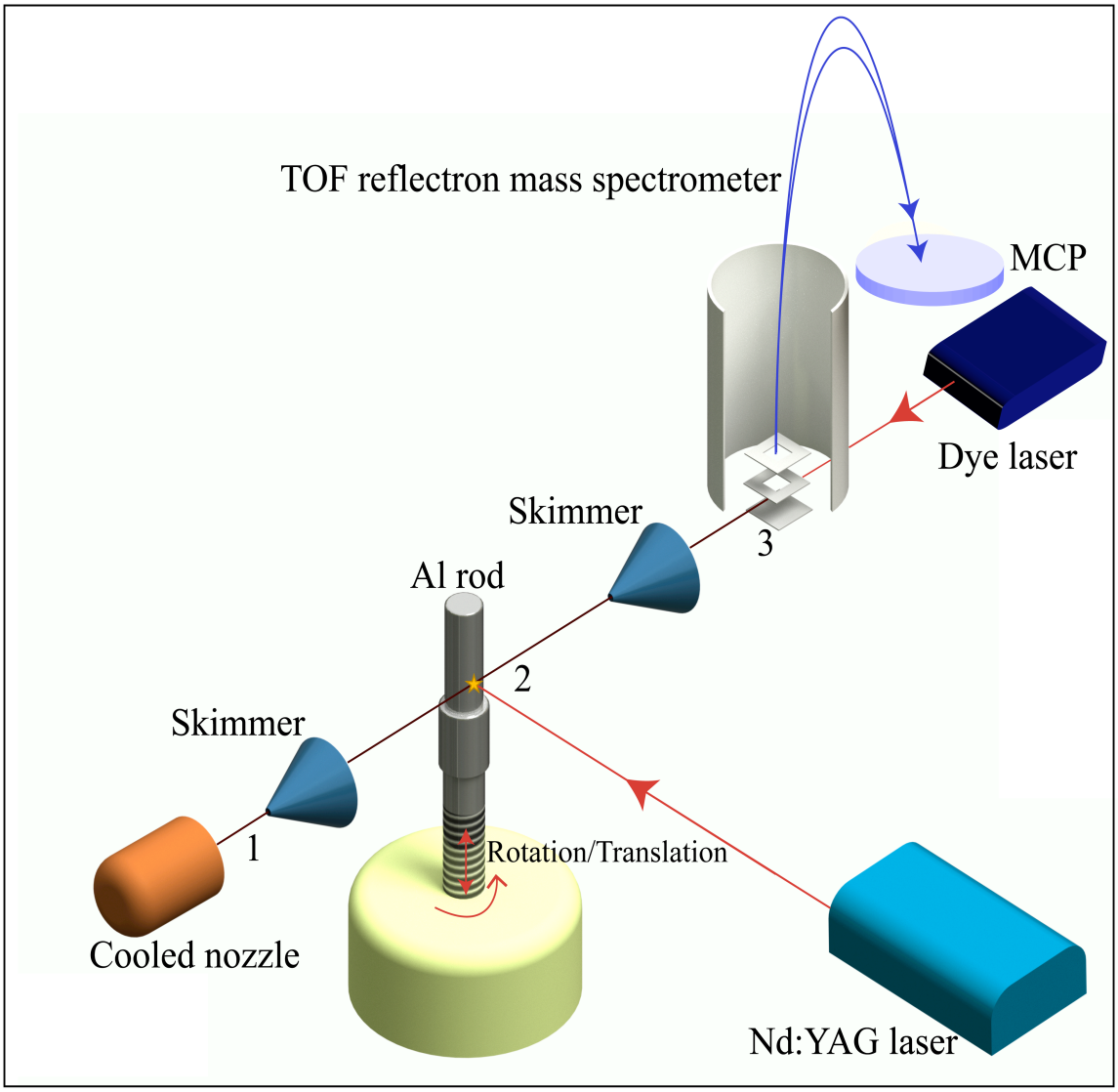
TOF reflectron mass spectrometer
MCP
Dye laser
Skimmer
3
Al rod
2
Skimmer
1
Rotation/Translation
Cooled nozzle
Nd:YAG laser

Figure 2.

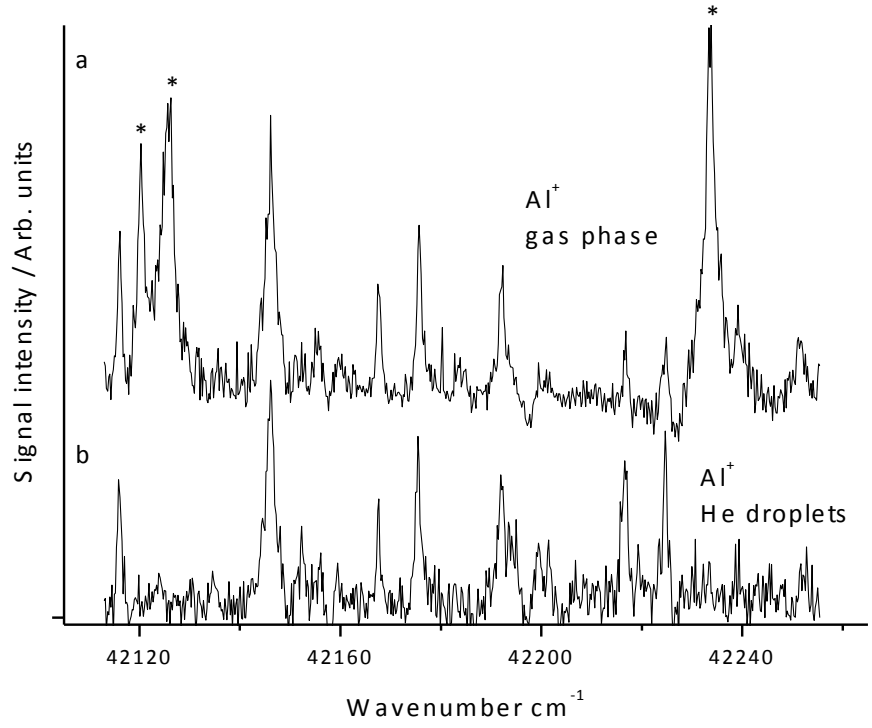
a
b
*
*
*
Al+
gas phase
Al+
He droplets
Signal intensity / Arb. units
42120
42160
42200
42240
Wavenumber cm-1

Figure 3.

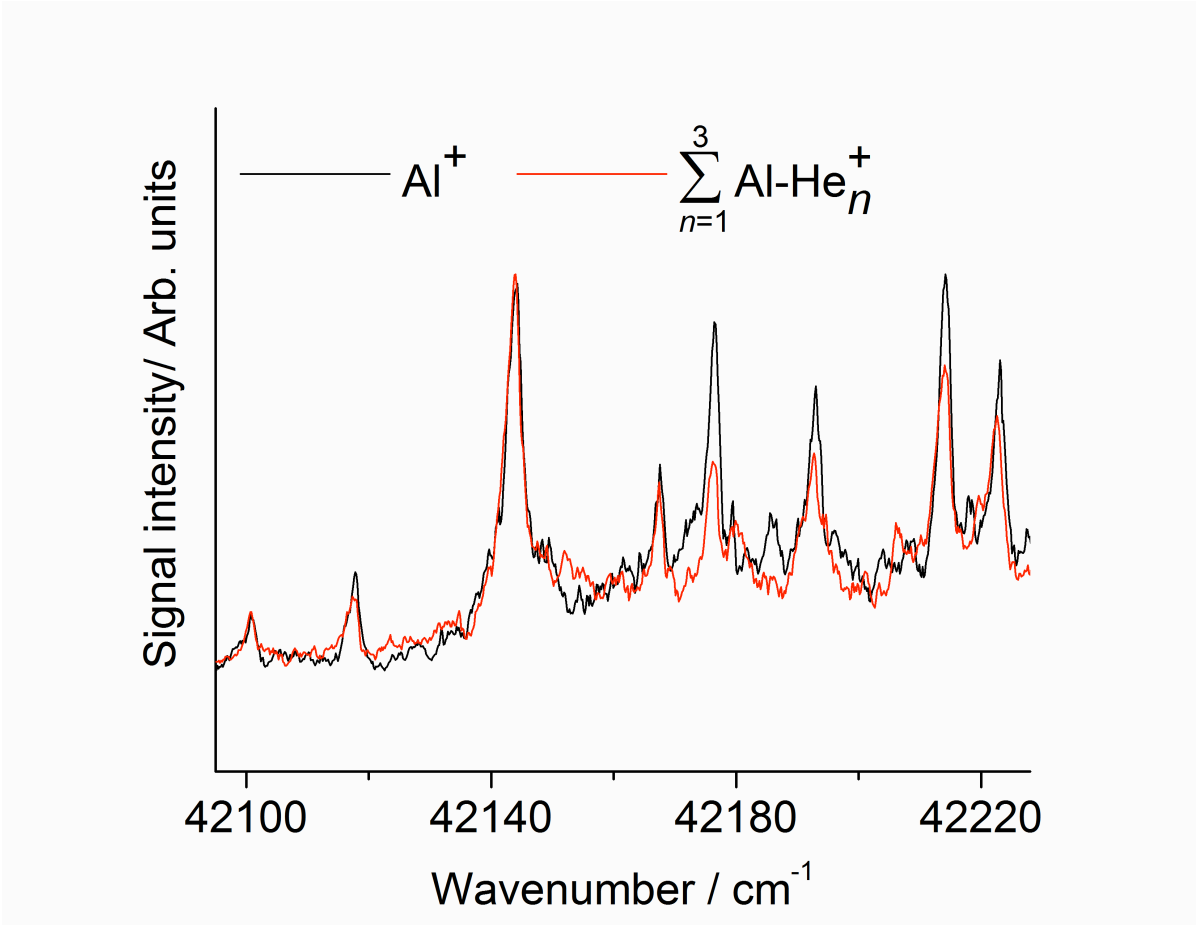
Al+
3
∑ Al-Hen+
n=1
Signal intensity/ Arb. units
42100
42140
42180
42220
Wavenumber / cm-1

Figure 4

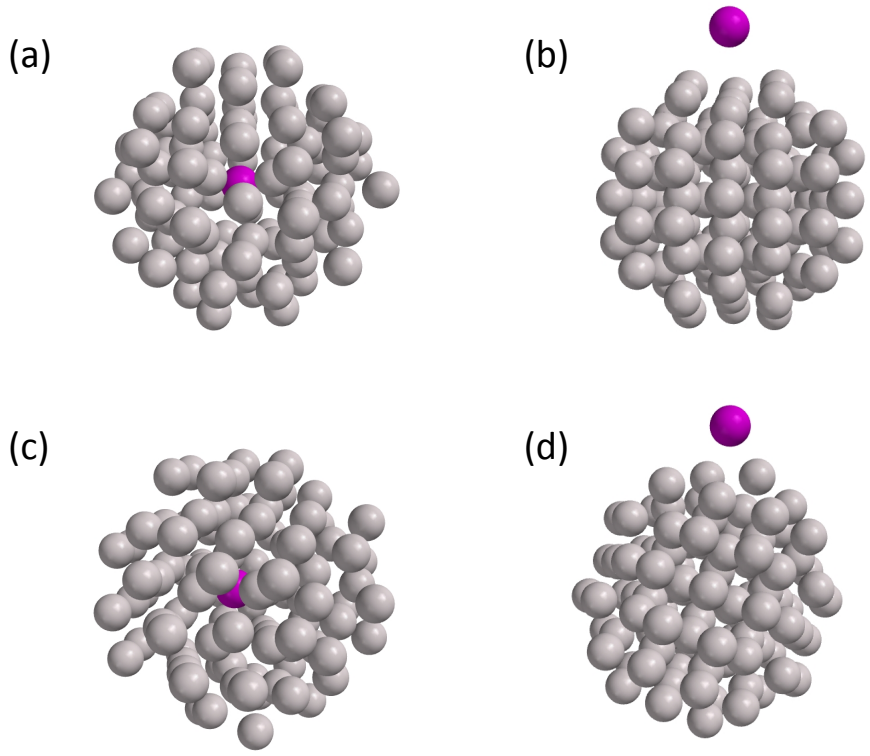

Table 1. Summary of electronic transitions recorded from the photoionization of metastable aluminium atoms in association with helium nanodroplets. All energies are in cm^{-1} and g.p. refers to gas phase.

Initial state $3s3p^2$	Final state $3s3p(^3P^0)3d$	Angular momentum states		Initial g.p. energy	Final g.p. energy	He droplet transition energy	Shift (He - g.p.)	He line width
		J_i	J_f					
^4P	$^4D^o$	1/2	3/2	29020.41	71244.17	42223.08	-0.68	2.78
^4P	$^4D^o$	1/2	1/2	29020.41	71235.25	42214.21	-0.63	2.91
^4P	$^4D^o$	3/2	5/2	29066.96	71260.55	42192.96	-0.63	4.66
^4P	$^4D^o$	3/2	3/2	29066.96	71244.17	42176.51	-0.70	1.78
^4P	$^4D^o$	3/2	1/2	29066.96	71235.25	42167.51	-0.78	1.41
^4P	$^4D^o$	5/2	7/2	29142.78	71286.40	42143.83	0.21	2.27
^4P	$^4D^o$	5/2	5/2	29142.78	71260.55	42117.86	0.09	2.06
^4P	$^4D^o$	5/2	3/2	29142.78	71244.17	42100.78	-0.61	1.35
^4P	$^4P^o$	5/2	3/2	29142.78	72250.53	43107.39	-0.36	1.91
^4P	$^4P^o$	3/2	3/2	29066.96	72250.53	43181.88	-1.69	1.65
^4P	$^4P^o$	3/2	1/2	29066.96	72277.75	43208.95	-1.84	1.21
^4P	$^4P^o$	1/2	3/2	29020.41	72250.53	43226.71	-3.41	1.23
^4P	$^4P^o$	1/2	1/2	29020.41	72277.75	43253.83	-3.51	1.37

Table 2. Equilibrium inter-nuclear separation (R_{min}) and well depth (ε) for Al-He_n clusters in the excited quartet state derived from CCSD(T)/d-aug-cc-pVQZ calculations.

Cluster	State	Al configuration	R_{min}(Å)	ε(cm^{-1})	ε/*n* (cm^{-1})
Al-He_1	$1^4\Pi$	$[Ne]3s^13p_x^1p_z^1$ $[Ne]3s^13p_y^1p_z^1$	5.38	4.8	4.8
	$1^4\Sigma$	$[Ne]3s^13p_x^1p_y^1$	2.44	173.9	173.9
Al-He_2	$1^4\Pi_u$	$[Ne]3s^13p_x^1p_z^1$ $[Ne]3s^13p_y^1p_z^1$	5.35	8.6	4.3
	$1^4\Sigma_u^-$	$[Ne]3s^13p_x^1p_y^1$	2.60	302.3	151.1
Al-He_4		$[Ne]3s^13p_x^1p_y^1$	2.65 (2,z) 5.43 (2,x)	266.4	66.6
[a]Al-He_6		$[Ne]3s^13p_x^1p_y^1$	2.68 (2,z) 5.39 (4,xy)	247.7	41.3
[b]Al-He_{98}	centre	$[Ne]3s^23p^1$ g.s[c]	3.76	1293	-
Al-He_{98}	surface	$[Ne]3s^23p^1$ g.s	4.41	1285	-
Al-He_{98}	centre	$[Ne]3s^13p^2$ e.s[d]	[e]2.94	1244	-
Al-He_{98}	surface	$[Ne]3s^13p^2$ e.s	[e]3.11	1327	-

[a] The results for Al-He_6 have been derived from CCSD(T)/d-aug-cc-pVTZ calculations.

[b] All calculations on Al-He_{98} clusters are at the RI-MP2/6-31++G* level of theory.

[c] Ground state

[d] Excited state

[e] Most closely associated with a He single atom.

References

1. K. B. Whaley, Int. Rev. Phys. Chem. **13**, 41 (1994).

2. J. P. Toennies and A. F. Vilesov, Annu. Rev. Phys. Chem. **49**, 1 (1998).

3. F. Stienkemeier and A. F. Vilesov, J. Chem. Phys. **115**, 10119 (2001).

4. J. Tiggesbäeumker and F. Stienkemeier, Phys. Chem. Chem. Phys. **9**, 4748 (2007).

5. F. Ancilotto, P. B. Lerner, and M. W. Cole, Low Temp. Phys. **101**, 1123 (1995).

6. F. Stienkemeier, J. Higgins, C. Callegari, S. I. Kanorsky, W. E. Ernst, and G. Scoles, Z. Phys. D **38**, 253 (1996).

7. F. Stienkemeier, F. Meier, and H. O. Lutz, J. Chem. Phys. **107**, 10816 (1997).

8. F. Stienkemeier, F. Meier, and H. O. Lutz, Eur. Phys. J. D **9**, 313 (1999).

9. J. Reho, U. Merker, M. R. Radcliff, K. K. Lehmann, and G. Scoles, J. Chem. Phys. **112**, 8409 (2000).

10. A. Hernando, R. Pi. M. Mayol, M. Barranco, F. Ancilotto, O. Bunermann and F. Stienkemeier, J. Phys. Chem. A **111**, 7303 (2007).

11. Y. Ren and V. V. Kresin Phys. Rev. A **76**, 043204 (2007).

12. J. Navarro, D. Mateo, M. Barranco, and A. Sarsa, J. Chem. Phys. **136**, 054301 (2012).

13. F. Lackner, J. Poms, G. Krois, J. V. Pototshnig, and W. E. Ernst, J. Phys. Chem. A **117**, 11866 (2013).

14. M. Koch, A. Kautsch, F. Lackner, W. E. Ernst, J. Phys. Chem. A **118**, 8373 (2014).

15. F. Stienkemeier, J. Higgins, W. E. Ernst, and G. Scoles, Phys. Rev. Lett. **74**, 3592 (1995).

16. J. Higgins, W. E. Ernst, C. Callegari, J. Reho, K. K. Lehmann, G. Scoles, and M. Gutowski, Phys. Rev. Lett. **77**, 4532 (1996).

17. J. Higgins, C. Callegari, J. Reho, F. Stienkemeier, W. E. Ernst, M. Gutowski, and G. Scoles, J. Phys. Chem. A **102**, 4952 (1998).

18. A. Przystawik, P. Radcliffe, S. Göde, K. H. Meiwesr-Broer, J. Tiggesbäumker, J. Phys. B **39**, S1183 (2006).

19. NIST http://www.nist.gov (2007).

20. K. Borje, K. B. S. Eriksson, and H. B. S. Isberg, Ark. för Fys. **23**, 527 (1963).

21. V. Vujnović, K. Blagoev, C. Fürböck, T. Neger, and H. Jäger, A&A **388**, 704 (2002).

22. A. Bartelt, J. D. Close, F. Federmann, K. Hoffmann, N. Quaas, and J. P. Toennies, Z. Phys. D **39**, 1 (1997).

23. J. H. Reho, U. Merker, M. R. Radcliff, K. K. Lehmann, and G. Scoles, J. Phys. Chem. A **104**, 3620 (2000).

24. T. Kinoshita, K. Fukuda, T. Matsuura, and T. Yabuzaki, Phys. Rev. A **53**, 4054 (1996).

25. A. Wucher, W. Berthold, H. Oechsner, and K. Franzreb, Phys. Rev. A **49** 2188 (1994) and references there in.

26. A. Hofer, P. Moroshkin, D. Nettels, S. Ulzega, and A. Weis, Phys. Rev. A **74** 032509 (2006).

27. J. Reho, J. Higgins, C. Callegari, K. K. Lehmann, and G. Scoles, J. Chem. Phys. **113** 9686 (2000).

28. J. Reho, J. Higgins, C. Callegari, K. K. Lehmann, and G. Scoles, J. Chem. Phys. **113** 96941 (2000).

29. C. P.Schulz, P. Claas, and F. Stienkemeier, Phys. Rev. Lett. **87**, 153401 (2001).

30. F. Federmann, K. Hoffmann, N. Quaas, and J. D. Close, Phys. Rev. Lett. **83** 2548 (1999).

Supplementary Information

Metastable aluminium atoms floating on the surface of helium nanodroplets.

Jay Jeffs[1], Nicholas A. Besley[1] and Anthony J. Stace[1*]
Gautam Sarma[2], Ethan M. Cunningham[2], Adrian Boatwright[2], Shengfu Yang[2], and Andrew M. Ellis[2]
[1]*Department of Physical Chemistry, School of Chemistry, The University of Nottingham, University Park, Nottingham NG7 2RD, U.K.*
[2]*Department of Chemistry, University of Leicester, Leicester LE1 7RH, U.K.*

Details of the experiment

Two instruments were employed in these experiments. In apparatus I (Nottingham; a schematic is shown in Fig. S1) a beam of helium nanodroplets was produced by the supersonic expansion of ultra-pure helium (6N) through a 5 μm diameter orifice at an inlet temperature and pressure of 9 K and 10 bar, respectively [1]. Downstream from the orifice the droplet beam was collimated successively by 0.5 mm and 2 mm diameter skimmers before passing between the repeller plates of a reflectron time of flight mass spectrometer (ReTOF) where photoionization took place. Ionization was achieved *via* resonant and non-resonant photoionization using the pulsed (10 Hz) output from a frequency doubled dye laser (Sirah Cobra-Strech). Typical energies were measured to be in the region of ~1.5×10^5 W cm^{-2} per pulse across the available wavelength range. To record ion intensities as a function of wavelength, time gated ion signals from microchannel plates were fed to an ion counting system (Stanford Research Inc. SR400). For most of the optical spectra reported below ion signals were counted for 300-600 laser shots per step in wavelength, the exact number depending on signal strength. The minimum step size used was 0.2 cm^{-1}, although this varied considerably according to the spectral width of the electronic transition under consideration. At 250 nm the linewidth of the laser was 0.15 cm^{-1}.

Three laser vaporisation sources of metal atoms were constructed to introduce ground and excited state atoms into the experiment [2,3]. At Nottingham the source consisted of an aluminium rod mounted on a stepper motor and located 6-10 mm downstream of the expansion orifice. Ablation was achieved by focussing the 532 nm output from a 10 Hz Nd:YAG laser (average power 10mJ pulse^{-1}) and material from the plume was captured in the expanding helium beam during droplet formation. Fig. S 2 shows a short section of a time-of-flight mass spectrum recorded in the region of Al^+ (m/z = 27) where, in addition to a strong bare metal ion signal there are weaker signals corresponding to $AlHe_n^+$ clusters for *n* in the range 1-8, as well as Al_2^+ and Al_3^+. Examples of temporal profiles recorded for pulsed resonant and non-resonant Al^+ and $AlHe^+$ photoionization signals are shown in Fig. S 3, where a FWHM of 80 -100 μs results from a combination of the spatial length of the droplet beam exposed to the metal plume and the velocity spread of the beam. The actual time delay between the ablation laser pulse and arrival of the peak maximum at the ReTOF corresponds to a beam velocity of ~300 m s^{-1}, which equates well with a calculated terminal velocity, ν, for supersonic expansion [$\nu = 5kT_0/m_{He}$] from a nozzle at a temperature of T_0. The mean droplet size in these experiments is estimated to be between 10^3 and 10^4 He atoms [4]. A second separate apparatus (Leicester, apparatus II, a schematic is shown in Fig. S 4), operating at a temperature and pressure of 6 K and 10 bar, respectively, produced droplets with a mean size of ~ 10^4 atoms and had an ablation source positioned *after* the first skimmer. In this source the helium droplets were already formed when they interacted with aluminium atoms ablated at 1032 nm.

On apparatus I, the signal to noise ratio for the capture and ionization of Al in helium droplets was optimised in a series of experiments performed under different conditions of stagnation pressure and ablation source position. Using two of the spectral transitions identified in Table 1, the intensity of the Al^+ photoion was monitored as a function of

stagnation pressure with the expansion nozzle temperature, T_0, held constant and the rod positioned 10 mm from the beam axis. The most notable observation was that at high pressures (~20 bar), which should produce the largest helium droplets, the Al^+ signal was at its lowest. The experiments also showed evidence of a slight variation in response from the two electronic transitions as a function of nozzle pressure. From this study it was determined that optimum pick-up of aluminium atoms was achieved with a nozzle pressure of ~ 10 bar. At pressures below this value the nozzle orifice became increasingly susceptible to blockages caused by ablated metal.

A second series of experiments measured variations in signal intensity as a function of ablation rod distance from the droplet beam axis. The most intense signal was achieved with the rod placed 12 mm from the beam axis. As expected, larger distances led to a drop in intensity due to a reduced Al atom density in the ablation plume as it expands from the rod. However, positions < 12 mm also gave a significant drop in signal intensity, and this was attributed to the high initial velocity and density of the plume destroying the droplets. Evidence to support this proposal came from measurements using the single ion monitoring facility on the quadruple mass spectrometer, where the intensity of He_2^+ generated by electron impact was recorded as a function of time using a 10 Hz trigger from the ablation laser. For rod distances below 5 mm scattering by the ablation plume depleted the He_2^+ signal linearly with distance, until at 0.5 mm when the ion signal disappeared completely.

A second ablation target on apparatus I was located close to the ion source of the ReTOF mass spectrometer and provided bare atoms that could be photoionized for the purposes of both acting as calibration points and as a means of separately identifying excited states produced as a consequence of the ablation process. This source has been constructed using a metal disk mounted level with the centre line of the droplet beam and equidistant between, but external to, the repelling and focusing plates of the ReTOF. The disk was

attached to a stepper motor on an externally adjustable position mount, which facilitated control of the distance of the disk from the centre of the ion source. The mount was earthed to prevent space charge distortion of the repelling voltages. What most distinguishes the ReTOF gas phase spectrum (upper trace in Fig. S 5) from that recorded in the presence of the helium droplets (lower trace in Fig. S 5) is the appearance in the former of three clearly identifiable strong lines, a pair near ~ 42130 cm^{-1} and another at ~ 42230 cm^{-1}, which disappear completely in the latter due to a spectral shift from their association with helium droplets. These peaks can be assigned as due to multi-photon transitions from the $3s^2 3p(^2P^o)$ electronic ground state to the ionization continuum of Al *via* an intermediate $3s^2 4d(^2D)$ state, and they have been the subject of a detailed experimental and theoretical study by Scoles *et al.*[5]

Overall, our diagnostics of the metal(M)-doped helium droplets closely match those used by other groups where mass spectrometry has been used to monitor M^+ and M^+He_n ions following either metal ablation or metal atom pick-up from an effusive cell [2,3,6]. Aluminium ions formed during the ablation process are not able to enter the reflectron time-of-flight mass spectrometer because of the high positive potential on the repeller plate. The laser operating in conjunction with apparatus I has been calibrated with a wavemeter and that on the apparatus II calibrated with an optogalvanic cell. Experiments showed the intensities of the sharp spectral features in Fig. S 5 to vary linearly as a function of laser power.

Finally, Fig. SI 6 shows the result of an experiment where the temperature of the expansion nozzle has been gradually increased and at the same time transformed into an equivalent *average* droplet size using a scaling relationship [7]. A strong correlation between the appearance of the Al^+ signal and the presence of large droplets emerging from the nozzle is seen. From Fig. 3, there also appears to be a good match between the minimum size of droplet required to pick-up a metal atom and the number of helium atoms typically assumed to evaporate on capturing that metal atom, i.e. several hundred helium atoms [2].

Details of the theory

Potential energy curves have been computed for the interaction of ground ($3s^2 3p\ ^2D$) and excited state ($3s3p^2\ ^4P$, see below) aluminium atoms with 1 - 6 helium atoms in each of the configurations shown in Fig. S 7 (the structures shown are not intended to represent global minima). Coupled cluster theory with single and double excitations and perturbative triple excitations (CCSD(T)) in conjunction with large doubly augmented correlation consistent basis sets [8,9] has been used as implemented in the MOLPRO software package [10], and corrected for basis set superposition error at each point [11]. It is shown below that the level of theory adopted gives results that agree well with previous calculations on a ground state aluminium atom in association with small numbers of helium atoms [5]. Optimized structures and binding energies of ground and excited state aluminium atoms at the centre and surface of a 98 atom He cluster were calculated at the RI-MP2/6-31++G* level of theory. Starting structures for optimization were generated by placing Al atoms at both the centre of a cluster and above distinct binding sites on the surface. The resultant structures are shown in Fig. S 8.

We have calibrated the theory by showing how results calculated for ground state aluminium atoms in association with helium compare with those presented previously by Reho *et al*.[5]. Table S 1 shows the properties of minima on Al-He dimer potential energy curves that were calculated using restricted open-shell coupled cluster theory with single and double excitations with a perturbative treatment of triple excitations (CCSD(T)) for a range of doubly augmented correlation consistent basis sets. The counterpoise correction was used to correct for basis set superposition error at each point. Results are shown for the $1^2\Sigma$ and $1^2\Pi$ states that arise from the unpaired electron occupying a p orbital parallel or perpendicular to the inter-nuclear axis, respectively. As can be seen, the $1^2\Pi$ state is more strongly bound than the $1^2\Sigma$ state because, when the unpaired electron is in the $3p_z$ orbital, the

helium atom experiences a greater repulsion. In the $1^2\Pi$ state, the helium atom is much closer to the aluminium at the minimum and interacts more strongly with the atom. With the d-aug-cc-pV5Z basis set, the calculations predict well depths of 19.38 cm^{-1} and 3.72 cm^{-1} relative to the $Al(Ne3s^23p^1)$ + $He(1s^2)$ asymptote for the $1^2\Pi$ and $1^2\Sigma$ states, respectively. The equilibrium Al-Al separation of 3.95 Å for the $1^2\Pi$ state is significantly smaller than the value of 5.80 Å calculated for the $1^2\Sigma$ state. However, both data sets compare favourably with the results of Reho *et al.* [5] who reported values of 16.45 cm^{-1} with R_{min}= 4.12 Å for the $1^2\Pi$ state and 3.74 cm^{-1} with R_{min}= 5.10 Å for the $1^2\Sigma$ state using a Hartree-Fock with damped dispersion approach. The effects of spin-orbit coupling have not been considered in this work. While the $1^2\Pi$ and $1^2\Sigma$ states will interact through spin-orbit coupling, previous work [5] showed relatively little difference in the well depth and internuclear separation between the $1^2\Pi$ and $1^2\Pi_{1/2}$ and the $1^2\Sigma$ and $1^2\Sigma_{1/2}$ states.

The very large d-aug-cc-pV5Z basis set contains *h* functions for aluminium and *g* functions for helium and is not practical for investigating systems larger than the Al-He dimer. As Table S 1 shows, potential energy curves calculated with a d-aug-cc-pVQZ basis set give very similar results to those determined from the more accurate calculations, and so the former has been adopted for the larger $AlHe_n$ complexes. These data are shown in Table SI 2, where it can be seen that the calculated results for $Al\text{-}He_2$ are similar to those found for the dimer, with the $1^2\Pi$ state being more strongly bound. The equilibrium bond length is 4.00 Å, and the total binding energy is approximately double that of the dimer. As might be expected, the most stable $Al\text{-}He_4$ cluster has the four helium atoms lying in the xy plane with the unpaired electron occupying the $3p_z$ orbital. This state has a binding energy of 73.07 cm^{-1}, which when considered as an energy per helium atom, ε/n, is very close in value to the $1^2\Pi$ state of $Al\text{-}He_1$. $Al\text{-}He_6$ probably represents the most realistic model for a helium droplet, but for these calculations it was necessary to use the smaller d-aug-cc-pVTZ basis set. As Table

S 2 shows, if the unpaired electron occupies the $3p_z$ orbital, four strongly-bound atoms occupy the xy plane and have bond lengths with aluminium that are comparable to those seen previously for the $^2\Pi$ states of the dimer and trimer. The two helium atoms coordinated in the z-direction are more weakly bound and their average binding energy per atom is comparable to those of the $^2\Sigma$ states of the dimer and trimer.

To study how aluminium atoms are accommodated in larger He clusters is not tractable at the CCSD(T) level of theory and a computationally less expensive method is required. Consequently, the binding energies of He at the centre and surface of a 98 atom He cluster were computed using resolution of the identity second order Moller-Plesset perturbation theory (RI-MP2) with the 6-31++G* basis set and cc-pVDZ auxiliary basis set. The 98 atom cluster was chosen because it is large enough to have more than one layer of helium surrounding a aluminium atom at the centre and it is highly symmetric, with T_d symmetry. The structures of the clusters with aluminium in its ground and excited states were fully optimized with the aluminium atom at the centre and surface of the clusters. It is not possible to explore fully all possible sites for the aluminium atom and the starting structures for the optimization were generated by placing the aluminium at the centre of the cluster and at several distinct binding sites on the surface. The lowest energy structures are shown in Fig. SI 8 and these show a distinct difference between the ground and excited states. In the excited quartet state the aluminium atom is closely associated with one helium atom, while in the ground state the aluminium atom has several equidistant neighbours. This reflects the behaviour observed in the small clusters, where in its excited state the aluminium binds strongly to a helium atom with the aluminium-helium bond perpendicular to the two occupied p orbitals

References

1. A. Boatwright, N. A. Besley, S. Curtis, R. R. Wright, and A. J. Stace, J. Chem. Phys. **123**, 021102 (2005).

2. P. Claas, S. –O.Mende, and F. Stienkemeier, Rev. Sci. Inst. **74**, 4071 (2003).

3. M. Mudrich, B. Forkl, S. Muller, M. Dvorak, O. Bunermann, and F. Stienkemeier, Rev. Sci. Inst. **78**, 103106 (2007).

4. A. V. Kanaev, L. Museur, T. Laarmann, S. Monticone, M. C. Castex, K. von Haeften, and T. Moller, J. Chem. Phys. **115**, 10248 (2001).

5. J. H. Reho, U. Merker, M. R. Radcliff, K. K. Lehmann, and G. Scoles, J. Phys. Chem. A **104**, 3620 (2000).

6. M. Koch, A. Kautsch, F. Lackner, W. E. Ernst, J. Phys. Chem. A **118**, 8373 (2014).

7. A. V. Kanaev, L. Museur, T. Laarmann, S. Monticone, M. C. Castex, K. von Haeften, and T. Moller, J. Chem. Phys. **115**, 10248 (2001).

8. D. E. Woon, and T. H. Dunning Jr., J. Chem. Phys. **98**, 1358 (1993).

9. D. E. Woon, T. H. Dunning Jr., J. Chem. Phys. **100**, 2975 (1994).

10. MOLPRO, version 2008.1, a package of *ab initio* programs, H. –J. Werner *et al.*, see http://www.molpro.net.

11. S. F. Boys and F. Bernardi, Mol. Phys. **19**, 553 (1970).

Figure S 1

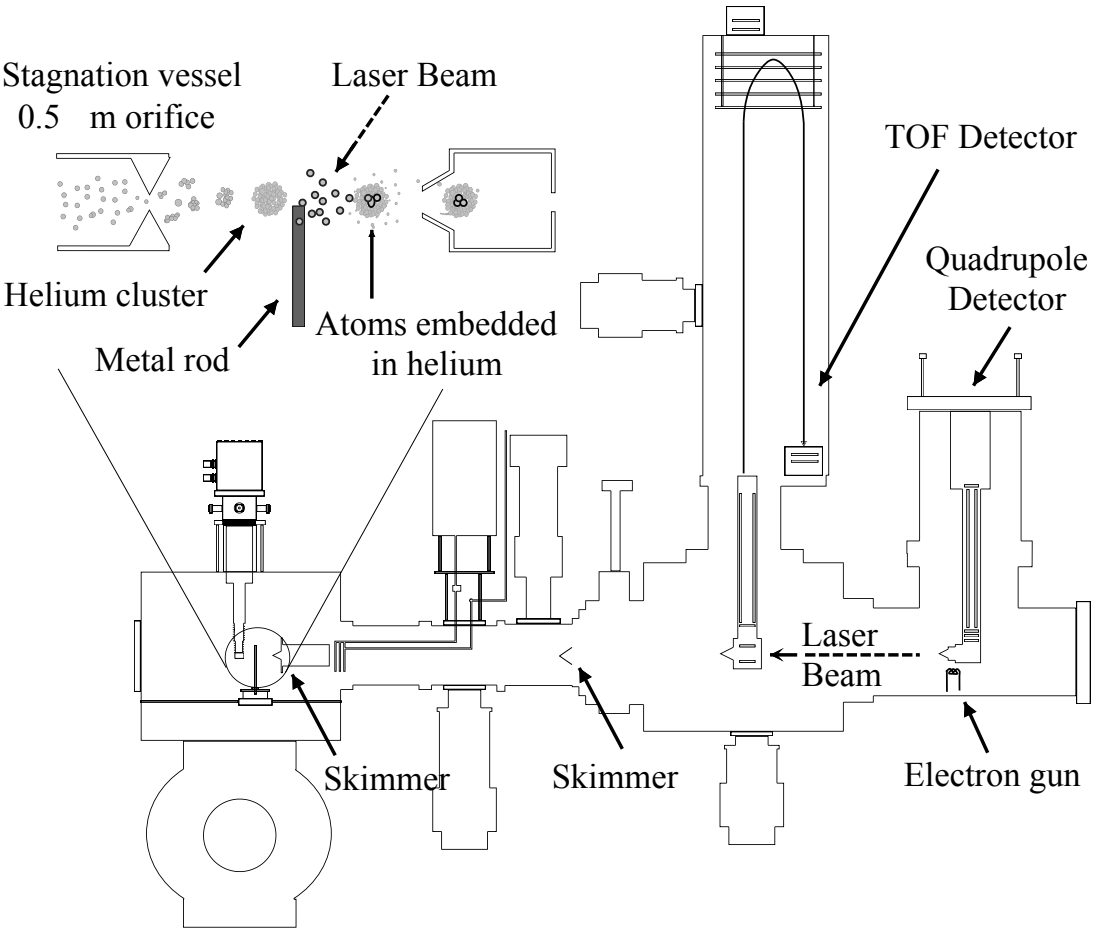

Schematic diagram of apparatus I (Nottingham) showing the positions of the helium droplet source, the ablation rod, the reflectron time-of-flight (ReTOF) mass spectrometer and the quadruple mass spectrometer.

Figure S 2

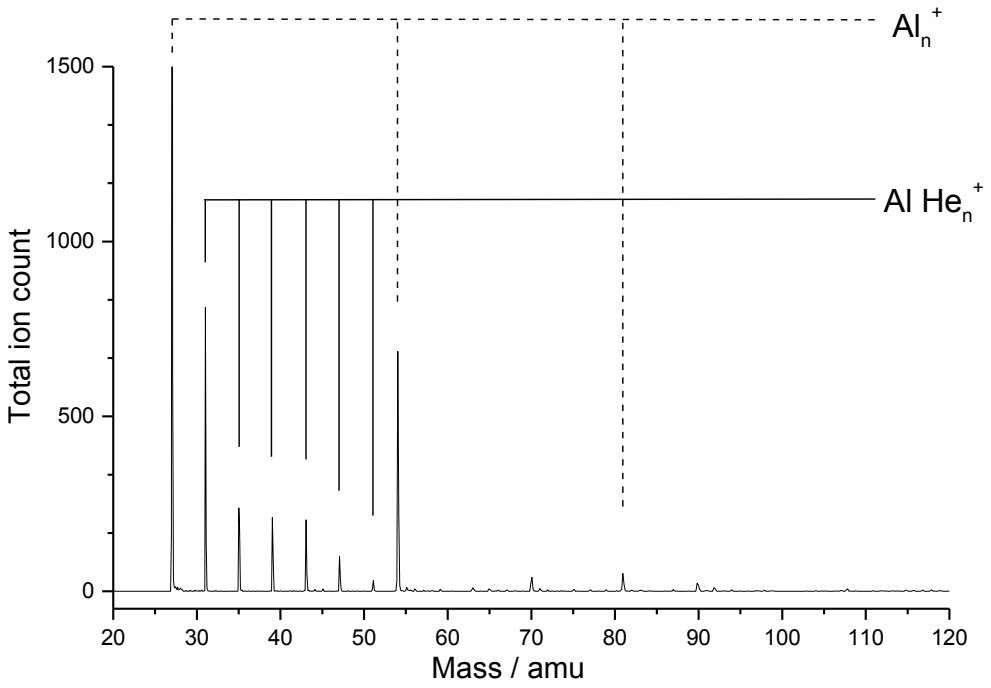

Photoionization mass spectrum recorded on the ReTOF of apparatus I at a photon energy of 43,500 cm^{-1}.

Figure S 3.

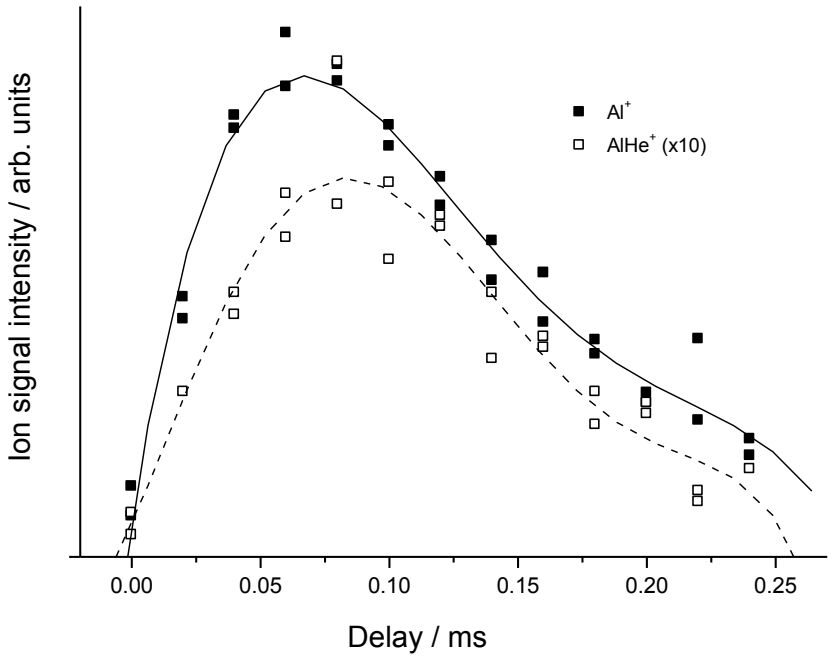

Temporal profiles recorded for Al^+ and $AlHe^+$ arriving at the detector of the ReTOF on apparatus I following the ablation of neutral atoms in to the path of a helium beam during droplet formation. The droplet beam was generated with a nozzle temperature of 9 K and a backing pressure of 10 bar, and the Al atoms were ionized with a photon energy of 42116 cm^{-1}.

Figure S 4.

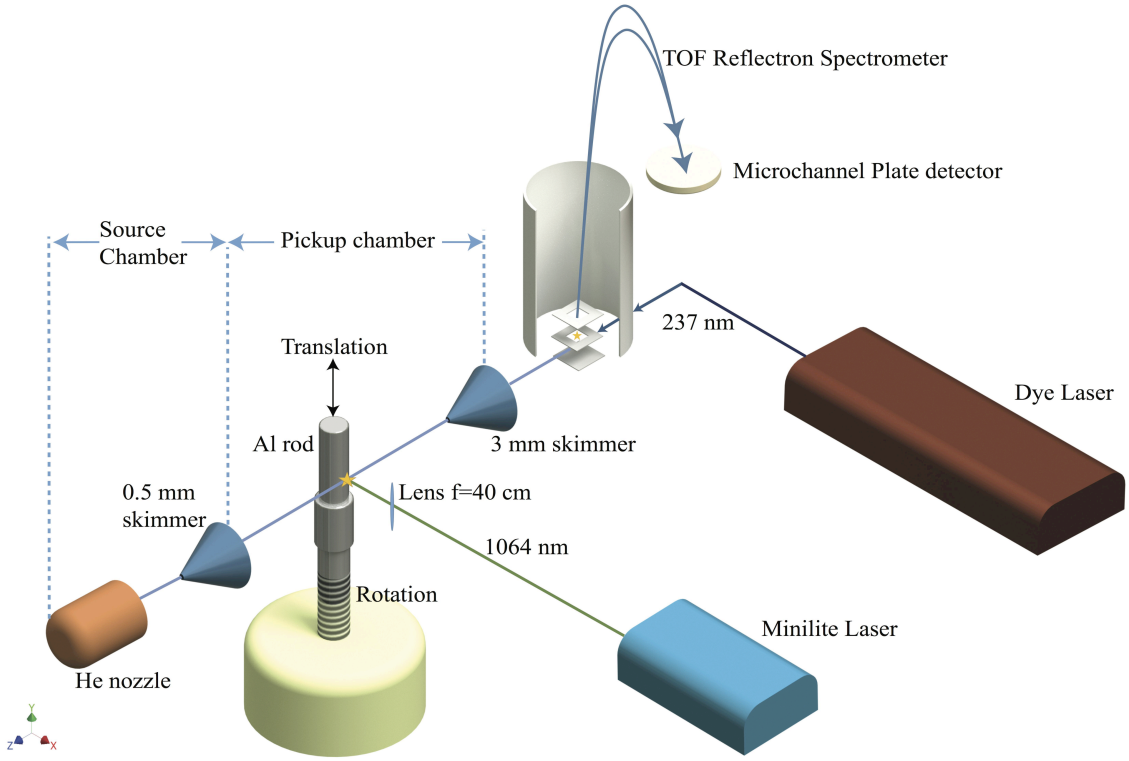

Schematic diagram of apparatus II (Leicester).

Figure S 5.

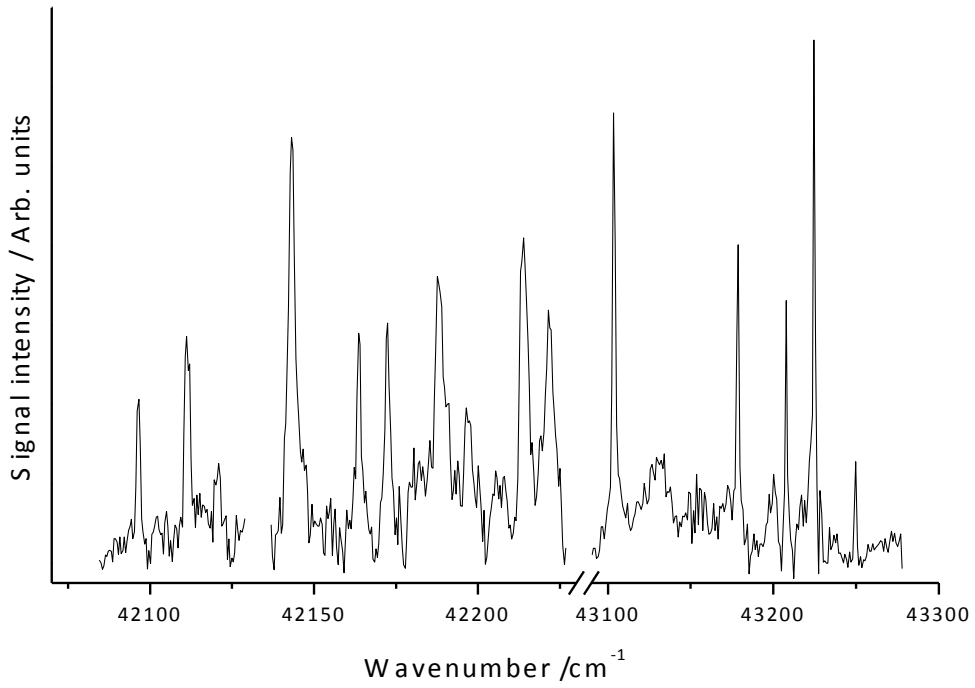

Photoionization spectrum of Al recorded following the ablation of Al atoms into a beam of nucleating helium atoms. The spectrum was recorded by monitoring the Al^+ signal in a time-of-flight mass spectrometer and the transitions are summarised in Table I and are assigned as originating from the $3s3p^2$ (^4P) metastable excited state of the Al atom.

Figure S 6

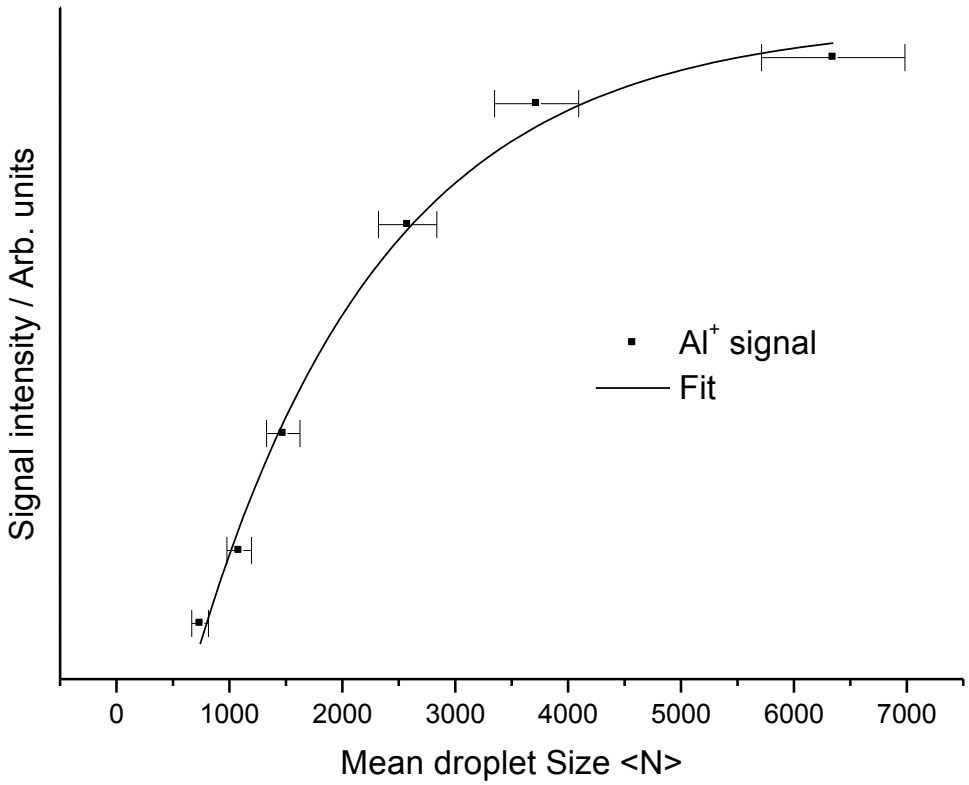

Intensity of the Al^+ signal originating from an excited state transition plotted as a function of the average number of helium atoms present in the droplets. The experiments were performed by varying the nozzle temperature and a scaling relationship was used to calculate <*N*>. The error bars reflect uncertainties in the sizes of the droplets.

Figure S 7.

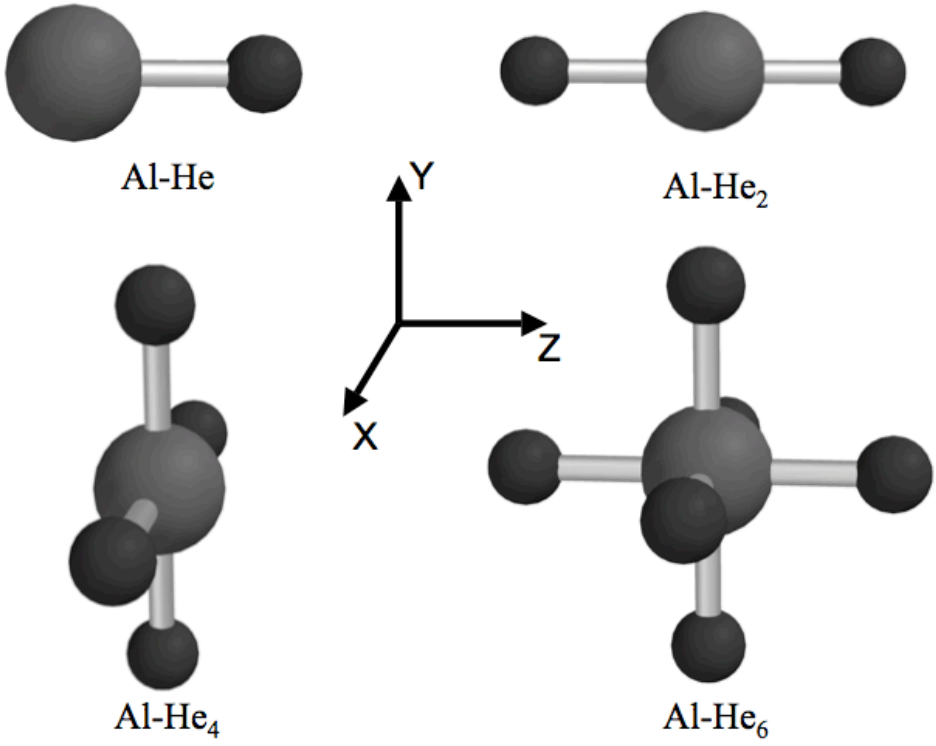

Calculated structures for $AlHe_n$ complexes with the aluminium atom in the electronic ground state.

Figure S 8.

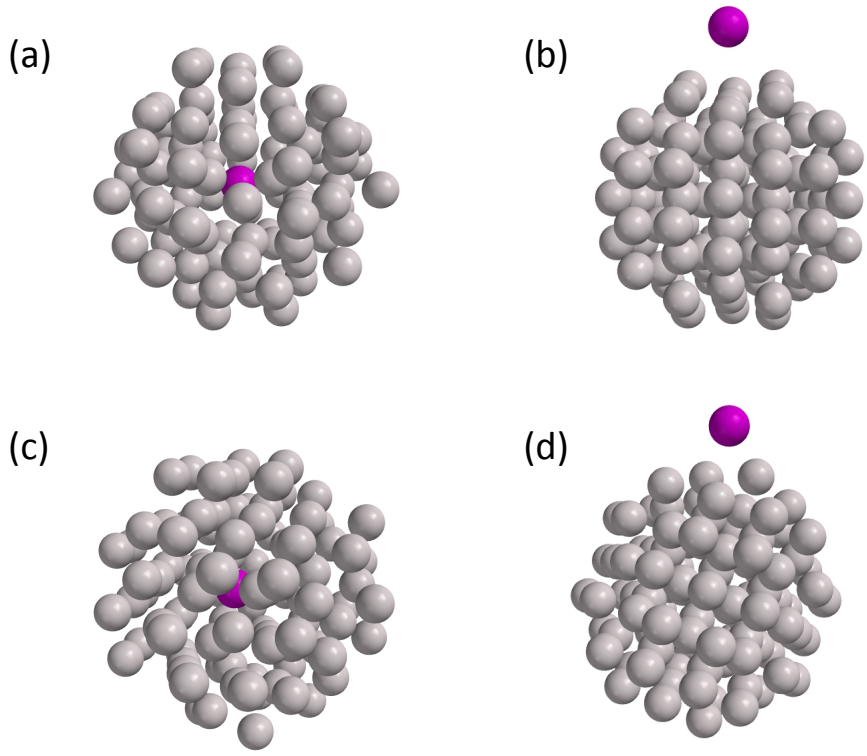

Optimized structures calculated for an aluminium atom at the centre and at the surface of a 98 atom helium cluster. (a) and (b) are for Al in the electronic ground state and (c) and (d) are for the $3s3p^2$ (^4P) excited state .

Table S 1. Computed equilibrium inter-nuclear separation (R_{min}) and well depth (ε) for Al-He dimer with Al in the ground $3s^2 3p$ electronic state.

	$1^2\Pi$		$1^2\Sigma$	
Basis Set	R_{min}(Å)	ε(cm^{-1})	R_{min}(Å)	ε(cm^{-1})
d-aug-cc-pVDZ	4.24	11.31	6.22	2.50
d-aug-cc-pVTZ	4.04	16.72	5.92	3.39
d-aug-cc-pVQZ	3.98	18.73	5.84	3.64
d-aug-cc-pV5Z	3.95	19.38	5.80	3.72

Table S 2. Computed CCSD(T)/d-aug-cc-pVQZ equilibrium inter-nuclear separation (R_{min}) and well depth (ε) for Al-He_n clusters in the ground $3s^2 3p$ electronic state.

Cluster	State	Al configuration	R_{min}(Å)	ε(cm^{-1})	ε/n (cm^{-1})
Al-He_1	$1^2\Pi$	$[Ne]3s^2 3p_x^1$	3.98	18.73	18.73
		$[Ne]3s^2 3p_y^1$			
	$1^2\Sigma$	$[Ne]3s^2 3p_z^1$	5.84	3.64	3.64
Al-He_2	$1^2\Pi_u$	$[Ne]3s^2 3p_x^1$	4.00	36.73	18.37
		$[Ne]3s^2 3p_y^1$			
	$1^2\Sigma_u^+$	$[Ne]3s^2 3p_z^1$	5.85	6.29	3.15
Al-He_4		$[Ne]3s^2 3p_z^1$	4.00(4)	73.07	18.29
[a]Al-He_6		$[Ne]3s^2 3p_z^1$	4.04 (4) 5.87 (2)	70.86	11.81

[a]CCSD(T)/d-aug-cc-pVTZ